J Nanopart Res (2013) 15:1331
DOI 10.1007/s11051-012-1331-5

RESEARCH PAPER

Synthesis, characterization, and electrochemical applications of multifunctional Fe_3O_4@C–Au nanocomposites

Shanhu Liu · Feng Lu · Yan Liu · Li-Ping Jiang · Jun-Jie Zhu

Received: 1 July 2012 / Accepted: 20 November 2012 / Published online: 16 December 2012

Abstract Fabrication of multifunctional nanocomposites that are simultaneously magnetic, stable, and biocompatible is critical for their application in bioanalysis but remains a challenge. In this study, Fe_3O_4@C–Au nanocomposites were prepared by a rapid microwave-hydrothermal procedure followed by the layer-by-layer assembly for this intention. The morphologies, composition, phase structures, and magnetic properties of the nanocomposites were well-characterized by field emission scanning electron microscopy, transmission electron microscopy, X-ray diffraction, X-ray photoelectron spectra, and superconducting quantum interference device. The nanocomposites have the sizes of about 200 nm in diameter. They integrate the advantages of the satisfactory stability of carbon shell, the good biocompatibility and conductivity of Au nanoparticles as well as the excellent magnetic properties of Fe_3O_4 core. Furthermore, a novel biosensor based on the multifunctional nanocomposites was fabricated after the immobilization of hemoglobin and the direct electrochemistry was studied. The proposed biosensor exhibits wide linear range, high sensitivity, good reproducibility, and stability. The presented multifunctional nanocomposites provide an alternative and effective matrix for the direct electrochemistry of proteins and might have potential applications in biosensing and drug delivery.

Keywords Nanocomposites · Magnetite · Gold · Electrochemistry

Introduction

Multifunctional nanomaterials are highly sought after in bioanalytic and biomedical sciences because of their potential applications in areas such as biosensing, drug delivery, diagnosis, and therapeutics (Dong et al. 2011; Wang et al. 2011; Mahmoudi et al. 2011; Bao et al. 2009; Shi et al. 2012; Xiao et al. 2012). In particular, introduction of practical functionality, such as biocompatibility, stability, and magnetic properties, into nanomaterials is desirable for many advanced techniques and clinical applications. For example, functionalized magnetic nanoparticles (NPs) were utilized to immobilize biomolecules and developed into magnetically controllable bioelectrochemical systems, while biocompatible Au NPs were used for

Electronic supplementary material The online version of this article (doi:10.1007/s11051-012-1331-5) contains supplementary material, which is available to authorized users.

S. Liu · L.-P. Jiang
Institute of Environmental and Analytical Sciences, College of Chemistry and Chemical Engineering, Henan University, Kaifeng 475004, People's Republic of China

S. Liu · F. Lu · Y. Liu · L.-P. Jiang (✉) · J.-J. Zhu
State Key Laboratory of Analytical Chemistry for Life Science, School of Chemistry and Chemical Engineering, Nanjing University, Nanjing 210093, People's Republic of China
e-mail: jianglp@nju.edu.cn

immunoassay applications (Zhou et al. 2012; Du et al. 2011; Xie et al. 2010).

Of the various magnetic nanomaterials reported in the literature for sensing purposes, iron oxides, mainly Fe_3O_4, have been most widely used because of their simple preparation, excellent magnetism, and biocompatibility (Song et al. 2012; Liu et al. 2011b; Liang et al. 2012; Chan et al. 2012; Balan et al. 2012). However, the problems of oxidation and aggregation limited applications of Fe_3O_4 NPs in biosensing (Liu et al. 2011d). To overcome these limitations, magnetic NPs often coated with some inert shells such as polymer and silica, as special immobilizing carrier of proteins are proposed. Recently developed amorphous carbon is another interesting coating material due to the hydrophilic surface and abundant amounts of –OH and $–COO^-$ groups, which enhances their dispersity in water and facilitates further coupling interaction with some guest molecules (Sun and Li 2004; Liu et al. 2011d).

Direct electrochemistry of proteins has attracted considerable attention because it provides fundamental knowledge of the redox behavior of proteins and helps to fabricate more effective biosensors and bioreactors (Zhang et al. 2008; Bao et al. 2008; Chen et al. 2009; Liu et al. 2011a). However, it is generally difficult for proteins to realize direct electron transfer on bare electrode surface due to the embedment of the electro active center or the denaturation of the protein adsorbed on the electrode surface (Zhang et al. 2007a; Xiao et al. 2009; Zhang et al. 2007b; Yang et al. 2008; Chen et al. 2008; Zhao et al. 2010). Different kinds of nanomaterials have been employed in the fabrication of biosensing interfaces to promote the electron transfer. Among them, biocompatible Au NPs, acting as a good conductive mediator to facilitate electron transfer, have been used and proven to be promising as the immobilization matrices for electrochemical biosensing (Guo et al. 2005; Cui et al. 2008a; Cai et al. 2006; Jha and Ramaprabhu 2010). In this study, multifunctional Fe_3O_4@C–Au nanocomposites were fabricated with magnetic core and carbon shell decorated with Au NPs. Comparing with the previous researches (Liu et al. 2011e), our method reported here is more general and facile to fabricate uniform nanocomposites. The fabrication process is shown in Scheme 1. Fe_3O_4 nanospheres were first prepared by a facile microwave-hydrothermal method, which is greatly advantageous for the preparation of uniform and monodisperse nanocrystals (Liu et al. 2011c). Then, carbon shell on Fe_3O_4 cores was achieved with glucose as a precursor via a microwave-hydrothermal process (step a). After that, Fe_3O_4@C core-shell nanospheres were functionalized with poly(diallyldimethylammonium chloride) (PDDA) to make the surface positively charged (step b) for the assembly of negatively charged AuNPs via the layer-by-layer assembly (step c). The Fe_3O_4@C–Au nanocomposites were further used for the loading of Hb to fabricate a biosensor (step d). Since Au NPs offer an optimized orientation and microenvironment for the immobilized protein (Cai et al. 2008), the immobilized Hb exhibit fast direct electron transfer and good electrocatalytic performance to H_2O_2 with high sensitivity and wide linear range from 10 to 350 μmol L^{-1}. The proposed method simplifies the immobilization methodology of proteins and the presented multifunctional nanocomposites offer a promising application in direct electrochemistry and biosensing.

Experimental section

Materials

Chloroauric acid ($HAuCl_4 \cdot 4H_2O$) and trisodium citrate and H_2O_2 were obtained from Shanghai Reagent Co., Ltd. PDDA (20 %, w/w in water, MW = 200,000–350,000) were purchased from Sigma-Aldrich. Glucose and the other reagents are of analytical reagent grade, purchased from Beijing Chemical Reagent Factory and used without further purification. PBS with various pHs was prepared by mixing stock solutions of NaH_2PO_4 and Na_2HPO_4, and then adjusting the pH with 0.1 mol L^{-1} NaOH and H_3PO_4. Millipore water (18.2 MΩ cm at 25 °C) was used throughout all experiments.

Preparation of Fe_3O_4@C nanospheres

Fe_3O_4 nanospheres were prepared according to our previous report (Liu et al. 2009). For the preparation of Fe_3O_4@C core-shell nanospheres, 0.1 g of Fe_3O_4 nanospheres were added to an aqueous solution of 0.3 mol L^{-1} glucose and sonicated for another 10 min. The mixed aqueous solution was treated at 170 °C and 180 psi for 30 min. The brown products were washed several times under sonication

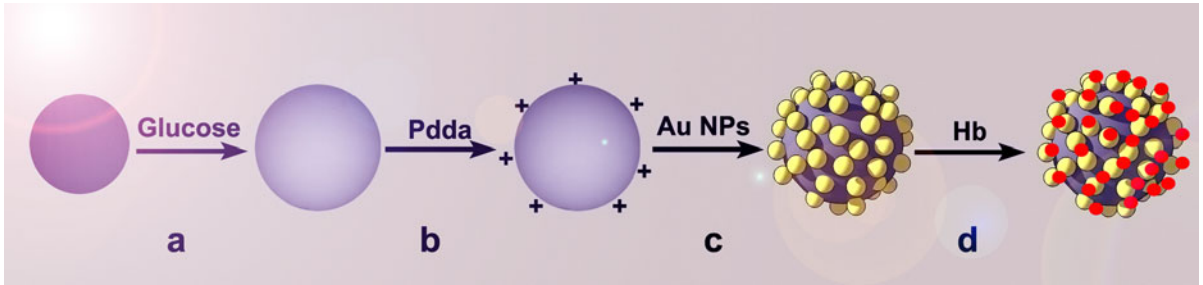

Scheme 1 Schematic illustration of the fabrication process of Fe_3O_4@C–Au–Hb biocomposites. **a** Carbon coating. **b** PDDA functionalization. **c** Decoration of Au NPs. **d** Assembly of Hb on the nanocomposites

with water and ethanol, and then dried under vacuum at room temperature before characterization and application.

Preparation of Fe_3O_4@C–Au–Hb biocomposites

For the preparation of Fe_3O_4@C–Au, Fe_3O_4@C nanospheres were first functionalized with PDDA. The nanospheres were dispersed into an aqueous solution of 0.20 % PDDA that contained 2.0×10^{-3} mol L^{-1} NaCl and the resulting dispersion was stirred for 20 min. Residual PDDA was removed by magnetic separation and the composites were rinsed with water at least three times. PDDA-functionalized nanospheres (0.05 g) were dispersed in 200 mL of Au colloid solution and sonicated for 20 min. AuNPs were prepared according to the literature by adding a sodium citrate solution to a boiling $HAuCl_4$ solution (Enustun and Turkevich 1963). And then the nanocomposites were collected by magnetic separation and washed several times under sonication with water and redispersed in 50 mL of 10 mmol L^{-1} PBS solutions (pH 6.0).

For the preparation of Fe_3O_4@C–Au-Hb, 5 mg of Fe_3O_4@C–Au nanocomposites was added to the Hb solution (5 mg mL^{-1} in 10 mmol L^{-1} PBS, pH 6.0) and shaken for 1 h for protein absorption. The biocomposites were then collected by magnetic separation and washed with PBS for three times.

Fabrication of the biosensor

The glass carbon electrode (GCE) was first polished with 1.0, 0.3, and 0.05 alumina slurry successively, sonicated in 1:1 nitric acid, acetone, and water and dried in air. 10 μL of the Fe_3O_4@C–Au–Hb suspension (about 10 mg/mL) was deposited on the pretreated GCE surface, and dried in a silica gel desiccator. 5 μL of Nafion solution (0.5 %) was added for encapsulation of the biocomposites. Finally, the electrode was left to dry at 4 °C overnight.

Characterization

Field emission scanning electron microscopy (FE-SEM) images were obtained using Hitachi S-4800 scanning electron microscope equipped with an X-ray energy dispersive spectroscopy (EDS) at an accelerating voltage of 20 kV. Transmission electron microscopy (TEM) images were taken using a JEOL JEM-2100 transmission electron microscope at an accelerating voltage of 200 kV. X-ray powder diffraction (XRD) measurements were performed on a Japan Shimadzu XRD-6000 X-ray powder diffractometer with Cu Kα radiation ($\lambda = 0.15418$ nm); a scanning rate of 0.05 deg/s was applied to record the patterns in the 2θ range of 20°–70°. X-ray photoelectron spectra (XPS) were obtained using a Thermo ESCALAB 250 electron spectrometer with 150 W monochromatized Al Kα radiation (1,486.6 eV). The binding energy of C1s level from contamination of saturated hydrocarbons at 284.8 eV was used as internal reference to calibrate the spectra. Electrochemical experiments were performed using a CHI660a workstation (Shanghai Chenhua, China) with a conventional three-electrode system, using a platinum wire as the auxiliary, a saturated calomel electrode as the reference and the modified GCE as the working electrode. Electrolyte solutions were deoxygenated before and during measurements.

Results and discussion

Characterization of Fe_3O_4@C–Au nanocomposites

The morphology and size distribution of Fe_3O_4@C–Au nanocomposites were investigated using SEM. As shown in Fig. 1a, Fe_3O_4@C–Au nanocomposites have a relatively narrow distribution with an average diameter of 200 nm, and show excellent monodispersity and uniform spherical shape on a large scale. There are numerous individual nanodots spreading along the nanospheres, indicating AuNPs were successfully decorated on the Fe_3O_4@C surface. AuNPs have an average size of 20 nm in diameter with a size distribution standard deviation of 4 nm (Supplementary Information, Fig. S1). The chemical composition of the nanocomposites was characterized by EDS and the corresponding elemental mapping was shown in Fig. 1b. Fe, O, and Au elements are homogeneously distributed along the whole nanospheres. The results indicate that high-density Au nanoparticles are efficiently decorated on the surface of nanospheres.

The crystal structures of Fe_3O_4 nanospheres and Fe_3O_4@C–Au nanocomposites were studied by XRD analyses. Figure 2 shows their XRD patterns. For the XRD pattern of Fe_3O_4 nanospheres (black line), the well-resolved diffraction peaks exhibit good crystallinity and all the peaks and positions match well with those from the JCPDS card (No. 75-0033) for a cubic magnetite. However, for the XRD pattern of the nanocomposites (red line), two new peaks at 38° and 65° appeared, corresponding to the (111) and (220) planes of Au nanoparticles, respectively. Calculations with the Debye–Scherrer formula for its strongest reflections (111) give the crystalline sizes of 26 nm, which is comparable to the SEM statistical value.

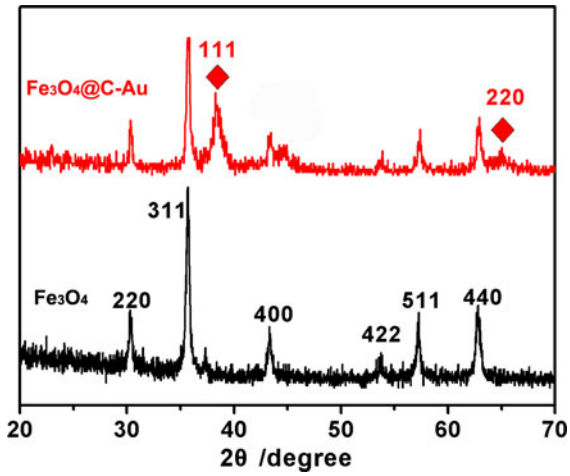

Fig. 2 XRD patterns of Fe_3O_4 nanospheres (*black line*) and Fe_3O_4@C–Au nanocomposites (*red line*). (Color figure online)

The incorporation of AuNPs on Fe_3O_4@C nanospheres is further demonstrated by XPS measurements (Fig. 3), which is considered as a powerful tool for identifying the chemical nature of the surface of nanomaterials. The photoelectron peaks at 700, 530, 285, and 85 eV, are accordingly assigned for Fe2p, O1s, C1s, and Au4f in the spectra, respectively. In the close-up view of the Fe2p and Au4f region (inset in Fig. 3), Fe 2p has the binding energy values of 710.8–724.6 eV for 2p3/2 and 2p1/2 and Au4f has the binding energy values of 83.6 and 87.4 eV for 4f7/2 and 4f5/2, respectively. These values are close to that reported before (Liu et al. 2011b; Cui et al. 2008b). Furthermore, the absence of shake-up satellites between the two Fe 2p peaks excludes the possible presence of g-Fe_2O_3, indicating that the Fe_3O_4 core is stable under the protection of carbon shell. These results indicated that AuNPs were successfully

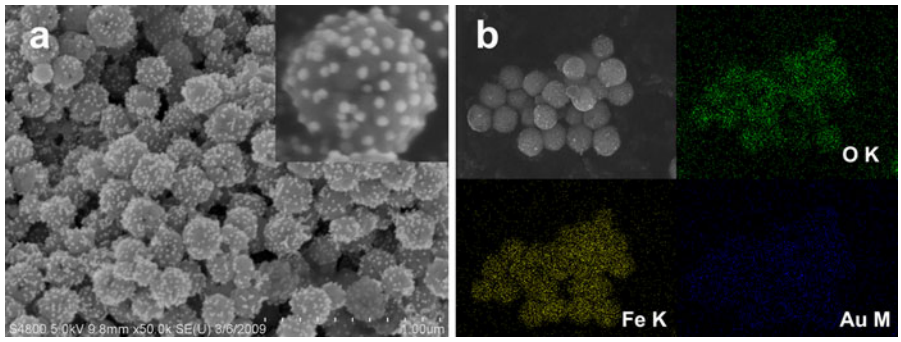

Fig. 1 SEM (**a**) and element mapping (**b**) images of Fe_3O_4@C–Au nanocomposites

immobilized on the outer surface of the nanocomposites in a well-dispersed way.

TEM analyses were performed to keep track of the fabrication of Fe_3O_4@C–Au nanocomposites and the results were shown in Fig. 4. Monodisperse and uniform Fe_3O_4 nanospheres with the diameter of about 160 nm were presented in Fig. 4a. After carbon coating, Fe_3O_4@C core-shell nanostructures were obtained and explicitly distinguished by the contrast difference of electron density as shown in Fig. 4b. The carbon shell has a thickness of about 20 nm around the nanospheres and is expected to protect the magnetic cores from erosion in acidic environments and provide abundant hydrophilic groups (i.e., –OH and $–COO^-$ groups) which could enhance their dispersity in water (Liu et al. 2011d). Followed by the functionalization of PDDA and the loading of AuNPs, Fe_3O_4@C–Au nanocomposites were obtained and many individual black nanodots appeared onto the core-shell nanospheres as shown in Fig. 4c, suggesting that AuNPs were dispersedly decorated on the surface of the carbon shell. PDDA was presumed to play a key role in the attachment of AuNPs; it acts as a bridge for the connection between AuNPs and carbon shell.

The assembly of AuNPs onto the surface of Fe_3O_4@C nanostructures was monitored by zeta potential (Supplementary Information, Fig. S2). As expected, Fe_3O_4@C in aqueous solution had a negative ξ-potential of −46 mV. After being attached with the cationic polyelectrolyte PDDA, Fe_3O_4@C nanostructures caused a reversal in ξ-potential to the positive value (+41 mV). After efficient adsorption of AuNPs, the ξ-potential of Fe_3O_4@C–Au nanocomposites decreased to +26 mV. This variation shows that these positive charges of the Fe_3O_4@C surface were neutralized by the negatively charged AuNPs via electrostatic interaction. The HR-TEM image in Fig. 4d further confirmed that AuNPs were attached on the carbon shell of Fe_3O_4@C nanostructures. In addition, the PDDA-functionalized Fe_3O_4@C nanostructures were also used to adsorb AgNPs and PdNPs (Supplementary Information, Fig S3), indicating that this method is a general route for the construction of Fe_3O_4@C-metal nanocomposites.

The magnetic properties of Fe_3O_4 nanospheres and Fe_3O_4@C–Au nanocomposites were studied using SQUID at room temperature. The saturation magnetization value is 82.9 and 47.1 emu g^{-1} for Fe_3O_4 nanospheres and Fe_3O_4@C–Au nanocomposites, respectively. From their respective enlarged curves shown in Fig. 5b, both of them reveal a weak ferromagnetism behavior with typical hysteresis loop; the remanence and coercivity are 6.1 emu g^{-1} and 52.7 Oe for the nanospheres and 4.6 emu g^{-1} and 63.8 Oe for the nanocomposites. The nanocomposites can be easily dispersed in water to form a black suspension and be drawn from the solution by an external magnetic field. They can be brought again back into the original solution by slightly agitating without external field. This implies that the nanocomposites can be used to separate and enrich certain biomolecules.

Electrocatalytic properties of Fe_3O_4@C–Au–Hb biocomposites

Since AuNPs provide an optimized orientation and microenvironment for the immobilized protein, the Fe_3O_4@C–Au nanocomposites were further used for

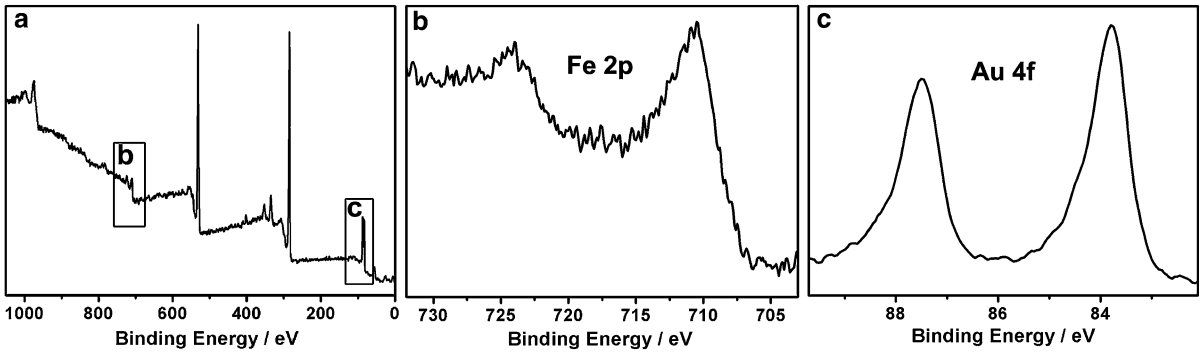

Fig. 3 XPS spectra of Fe_3O_4@C–Au nanocomposites **a**, high resolution XPS spectra of Fe2p **b** and Au4f **c**

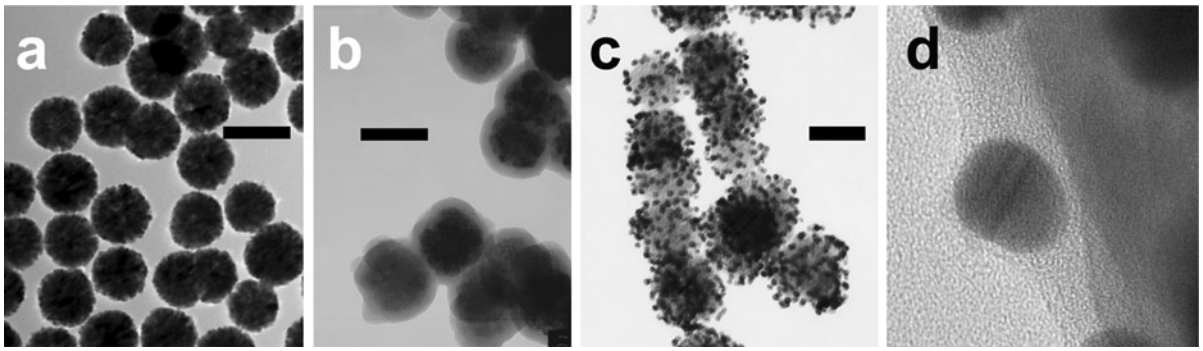

Fig. 4 TEM image of **a** Fe_3O_4 nanospheres, **b** Fe_3O_4@C core-shell nanostructures, **c** Fe_3O_4@C–Au nanocomposites (all the *scale bars* are 200 nm); and **d** HR-TEM image of Fe_3O_4@C–Au nanocomposites

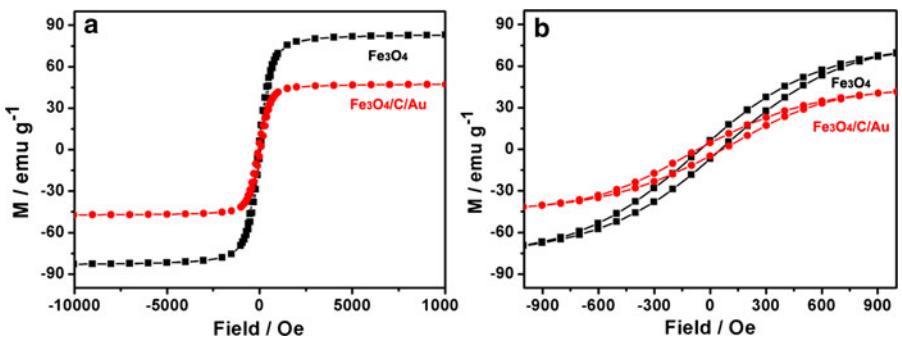

Fig. 5 **a** Room-temperature magnetization curves as a function of field for Fe_3O_4 nanospheres and Fe_3O_4@C–Au nanocomposites. **b** Enlarged curves around zero field with a *scale* ranging from −1,000 to 1,000 Oe

loading Hb to fabricate Fe_3O_4@C–Au–Hb biocomposites. By virtue of magnetic properties, the manipulation was facile and efficient. The biocomposites inherited the advantages from their parent materials and were expected to offer a favorable and biocompatible microenvironment for promoting the direct electron transfer between proteins and electrode surface (Bao et al. 2008; Chen et al. 2009; Zhang et al. 2007a; Xiao et al. 2009; Shan et al. 2009).

First, the dependence of the peak currents on the scan rates is illustrated in Fig. 6. The electrode modified with Fe_3O_4@C–Au–Hb biocomposites shows a pair of well-defined redox peaks. Furthermore, the reduction and oxidation peak currents increase linearly with the increase of scan rates from 20 to 300 mV s^{-1}. The results imply that the immobilized Hb on the surface undergoes a quasi-reversibly surface-controlled electron transfer process. According to Faraday's law, $Q = nFA\Gamma^*$, where Q can be obtained by integrating the reduction peak of Hb; F is Faraday constant and n and A stand for the number of electron transferred and the area of the electrode surface,

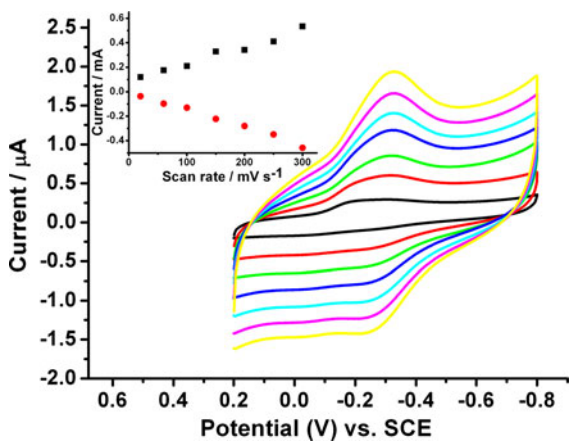

Fig. 6 Effect of scan rates on the cyclic voltammograms of Fe_3O_4@C–Au–Hb in pH 7.0 PBS with the scan rate of 20, 60, 100, 150, 200, 250, and 300 mV s^{-1} (from inner to outer). *Inset* plots of peak currents versus scan rates

respectively. The surface concentration of electro active Hb (Γ^*) at Fe_3O_4@C–Au–Hb modified GCE was estimated to be 5.3×10^{-11} mol cm^{-2}, which is

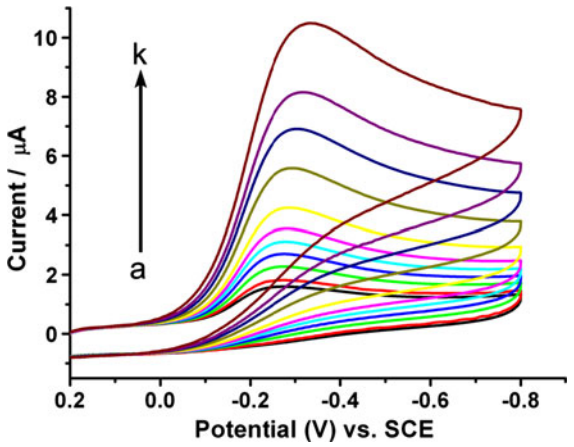

Fig. 7 CVs of Fe_3O_4@C–Au–Hb in 0.1 mol L^{-1} PBS 7.0 containing H_2O_2 (*a* 10, *b* 20, *c* 40, *d* 60, *e* 80, *f* 100, *g* 150, *h* 200, *i* 350, *j* 450, *k* 650 μmol L^{-1} respectively). The scan rate is 100 mV s^{-1}

larger than the theoretical monolayer coverage of Hb (ca. 1.89×10^{-11} mol cm^{-2}). This indicates saturated absorption of multilayered Hb in Fe_3O_4@C–Au nanocomposite matrix.

Since Hb has certain intrinsic peroxidase activity due to its close similarity with peroxidase, it can be employed to catalyze the reduction of hydrogen peroxide. Figure 7 displays cyclic voltammograms (CVs) in the presence of H_2O_2 at different concentrations. The reduction peak current increases linearly with increasing concentration of H_2O_2 in the range of 10–350 μmol L^{-1}, indicating that the immobilized Hb exhibits excellent electrocatalytic activity toward the reduction of H_2O_2. The linear regression equation is $y = 0.015x + 1.1191$. The relative standard deviation (R.S.D.) is 4.1 % for six successive measurements at 20 μM H_2O_2, showing the proposed biosensor possesses a good reproducibility. In addition, the stability of the Fe_3O_4@C–Au–Hb modified electrode was investigated by CVs in the presence of 20 μmol L^{-1} H_2O_2 after being stored for one month in 0.1 mol L^{-1} pH7.0 PBS at 4 °C. The biosensor retained 93 % of its original response, suggesting the acceptable operational stability of the proposed biosensor. These results indicate that the Fe_3O_4@C–Au–Hb modified electrode was very efficient for retaining high enzymatic activity and preventing enzyme leakage from the nanocomposite matrix, which was very significant for the development of novel biosensors in low-cost application.

Conclusions

In summary, we have developed a facile method to fabricate multifunctional Fe_3O_4@C–Au nanocomposites. The multifunctional nanocomposites not only simplify the manipulation process, but also facilitate direct electron transfer between redox active centers of protein and electrode surface. The immobilized Hb exhibited fast direct electron transfer and good electro catalytic performance to H_2O_2. The presented biosensor shows wide linear range, high sensitivity, good reproducibility, and stability. The multifunctional nanocomposites open a new avenue for immobilizing proteins and fabricating excellent electrochemical biosensor.

Acknowledgments We greatly appreciate the support of the National Natural Science Foundation of China (No. 21075061, 21105021) and the Natural Science Foundation of Jiangsu Province of China (BK2010363).

References

Balan V, Petrache I, Popa M, Butnaru M, Barbu E, Tsibouklis J, Verestiuc L (2012) Biotinylated chitosan-based SPIONs with potential in blood-contacting applications. J Nanopart Res 14(2):1–14

Bao SJ, Li CM, Zang JF, Cui XQ, Qiao Y, Guo J (2008) New nanostructured TiO_2 for direct electrochemistry and glucose sensor applications. Adv Funct Mater 18(4):591–599

Bao F, Yao J-L, Gu R-A (2009) Synthesis of magnetic Fe_2O_3/Au core/shell nanoparticles for bioseparation and immunoassay based on surface-enhanced Raman spectroscopy. Langmuir 25(18):10782–10787

Cai WY, Xu Q, Zhao XN, Zhu JH, Chen HY (2006) Porous gold–nanoparticle–$CaCO_3$ hybrid material: preparation, characterization, and application for horseradish peroxidase assembly and direct electrochemistry. Chem Mater 18(2):279–284

Cai WY, Feng LD, Liu SH, Zhu JJ (2008) Hemoglobin–CdTe–$CaCO_3$@polyelectrolytes 3D architecture: fabrication, characterization, and application in biosensing. Adv Funct Mater 18(20):3127–3136

Chan C, Gallard H, Majewski P (2012) Fabrication of amine-functionalized magnetite nanoparticles for water treatment processes. J Nanopart Res 14(4):1–11

Chen X, Fu CL, Wang Y, Yang WS, Evans DG (2008) Direct electrochemistry and electrocatalysis based on a film of horseradish peroxidase intercalated into Ni-Al layered double hydroxide nanosheets. Biosens Bioelectron 24(3): 356–361

Chen X, Zhang JJ, Xuan J, Zhu JJ (2009) Myoglobin/gold nanoparticles/carbon spheres 3-D architecture for the fabrication of a novel biosensor. Nano Research 2(3):210–219

Cui RJ, Huang HP, Yin ZZ, Gao D, Zhu JJ (2008a) Horseradish peroxidase-functionalized gold nanoparticle label for amplified immunoanalysis based on gold nanoparticles/carbon nanotubes hybrids modified biosensor. Biosens Bioelectron 23(11):1666–1673

Cui RJ, Liu C, Shen JM, Gao D, Zhu JJ, Chen HY (2008b) Gold nanoparticle-colloidal carbon nanosphere hybrid material: preparation, characterization, and application for an amplified electrochemical immunoassay. Adv Funct Mater 18(15):2197–2204

Dong W, Li Y, Niu D, Ma Z, Gu J, Chen Y, Zhao W, Liu X, Liu C, Shi J (2011) Facile synthesis of monodisperse superparamagnetic Fe_3O_4 Core@hybrid@Au shell nanocomposite for bimodal imaging and photothermal therapy. Adv Mater 23(45):5392–5397

Du D, Tao Y, Zhang W, Liu D, Li H (2011) Oxidative desorption of thiocholine assembled on core-shell Fe3O4/AuNPs magnetic nanocomposites for highly sensitive determination of acetylcholinesterase activity: an exposure biomarker of organophosphates. Biosens Bioelectron 26(10):4231–4235

Enustun BV, Turkevich J (1963) Coagulation of colloidal gold. J Am Chem Soc 85(21):3317–3328

Guo YG, Hu JS, Liang HP, Wan LJ, Bai CL (2005) TiO_2-based composite nanotube arrays prepared via layer-by-layer assembly. Adv Funct Mater 15(2):196–202

Jha N, Ramaprabhu S (2010) Development of Au nanoparticles dispersed carbon nanotube-based biosensor for the detection of paraoxon. Nanoscale 2(5):806–810

Liang C, Jing L, Shi X, Zhang Y, Xian Y (2012) Magnetically controlled bioelectrocatalytic system based on ferrocene-tagged magnetic nanoparticles by thiol-ene reaction. Electrochim Acta 69:167–173

Liu SH, Xing RM, Lu F, Rana RK, Zhu JJ (2009) One-pot template-free fabrication of hollow magnetite nanospheres and their application as potential drug carriers. J Phys Chem C 113(50):21042–21047

Liu S, Tian J, Wang L, Sun X (2011a) Microwave-assisted rapid synthesis of Ag nanoparticles/graphene nanosheet composites and their application for hydrogen peroxide detection. J Nanopart Res 13(10):4539–4548

Liu SH, Lu F, Jia XD, Cheng FF, Jiang LP, Zhu JJ (2011b) Microwave-assisted synthesis of a biocompatible polyacid-conjugated Fe_3O_4 superparamagnetic hybrid. Cryst Eng Comm 13(7):2425–2429

Liu SH, Lu F, Xing RM, Zhu JJ (2011c) Structural effects of Fe_3O_4 nanocrystals on peroxidase-like activity. Chemistry—A. Eur J 17(2):620–625

Liu Y, Zhou L, Hu Y, Guo C, Qian H, Zhang F, Lou XW (2011d) Magnetic-field induced formation of 1D Fe_3O_4/C/CdS coaxial nanochains as highly efficient and reusable photocatalysts for water treatment. J Mater Chem 21(45):18359–18364

Liu Y, Han T, Chen C, Bao N, Yu C, Gu H (2011e) A novel platform of hemoglobin on core-shell structurally Fe3O4@Au nanoparticles and its direct electrochemistry. Electrochim Acta 56(9):3238–3247

Mahmoudi M, Amiri H, Shokrgozar MA, Sasanpour P, Rashidian B, Laurent S, Casula MF, Lascialfari A (2011) Raman active jagged-shaped gold-coated magnetic particles as a novel multimodal nanoprobe. Chem Commun 47(37): 10404–10406

Shan CS, Yang HF, Song JF, Han DX, Ivaska A, Niu L (2009) Direct electrochemistry of glucose oxidase and biosensing for glucose based on graphene. Anal Chem 81(6): 2378–2382

Shi J, Tong L, Liu D, Yang H (2012) Fabrication, structure, and properties of Fe_3O_4@C encapsulated with YVO4:Eu3+ composites. J Nanopart Res 14(4):1–9

Song Y, He Z, Hou H, Wang X, Wang L (2012) Architecture of Fe_3O_4-graphene oxide nanocomposite and its application as a platform for amino acid biosensing. Electrochim Acta 71:58–65

Sun X, Li Y (2004) Colloidal carbon spheres and their core/shell structures with noble-metal nanoparticles. Angew Chem Int Ed 43(5):597–601

Wang C, Li J, Amatore C, Chen Y, Jiang H, Wang XM (2011) Gold nanoclusters and graphene nanocomposites for drug delivery and imaging of cancer cells. Angew Chem Int Ed 50(49):11644–11648

Xiao XL, Luan QF, Yao X, Zhou KB (2009) Single-crystal CeO_2 nanocubes used for the direct electron transfer and electrocatalysis of horseradish peroxidase. Biosens Bioelectron 24(8):2447–2451

Xiao D, Dramou P, He H, Pham-Huy L, Li H, Yao Y, Pham-Huy C (2012) Magnetic carbon nanotubes: synthesis by a simple solvothermal process and application in magnetic targeted drug delivery system. J Nanopart Res 14(7):1–12

Xie H-Y, Zhen R, Wang B, Feng Y-J, Chen P, Hao J (2010) Fe_3O_4/Au core/shell nanoparticles modified with Ni^{2+}–nitrilotriacetic acid specific to histidine-tagged proteins. J Phys Chem C 114(11):4825–4830

Yang J, Zhang RY, Xu Y, He PG, Fang YZ (2008) Direct electrochemistry study of glucose oxidase on Pt nanoparticle-modified aligned carbon nanotubes electrode by the assistance of chitosan-CdS and its biosensoring for glucose. Electrochem Commun 10(12):1889–1892

Zhang L, Zhang Q, Li JH (2007a) Layered titanate nanosheets intercalated with myoglobin for direct electrochemistry. Adv Funct Mater 17(12):1958–1965

Zhang L, Zhang Q, Lu XB, Li JH (2007b) Direct electrochemistry and electrocatalysis based on film of horseradish peroxidase intercalated into layered titanate nano-sheets. Biosens Bioelectron 23(1):102–106

Zhang JJ, Liu YG, Jiang LP, Zhu JJ (2008) Synthesis, characterizations of silica-coated gold nanorods and its applications in electroanalysis of hemoglobin. Electrochem Commun 10(3):355–358

Zhao HY, Xu XX, Zhang JX, Zheng W, Zheng YF (2010) Carbon nanotube-hydroxyapatite-hemoglobin nanocomposites with high bioelectrocatalytic activity. Bioelectrochemistry 78(2):124–129

Zhou H, Lee J, Park TJ, Lee SJ, Park JY, Lee J (2012) Ultrasensitive DNA monitoring by Au–Fe_3O_4 nanocomplex. Sens Actuators B: Chem 163(1):224–232